Int. J. Electrochem. Sci., 13 **(2018)** 7846 – 7858, doi: 10.20964/2018.08.06

International Journal of
ELECTROCHEMICAL
SCIENCE
www.electrochemsci.org

AC Susceptibility and Excess Conductivity Analysis of Cd Substituted $(Tl_{0.6}Bi_{0.4})Sr_2(Ca_{1-x}Cd_x)Cu_2O_{7-\delta}$ Superconductor

S.S.O. Farhat, R. Abd-Shukor[*]

School of Applied Physics, Universiti Kebangsaan Malaysia, 43600 Bangi, Selangor, Malaysia
[*]E-mail: ras@ukm.edu.my

Received: 16 March 2018 / *Accepted:* 10 May 2018 / *Published:* 5 July 2018

The effect of Cd on $(Tl_{0.6}Bi_{0.4})Sr_2(Ca_{1-x}Cd_x)Cu_2O_{7-\delta}$ **(**Tl-1212) superconductor is reported. Cd was chosen to partially replace Ca due to the single valence (+2) of both elements and this work is focused on the ionic radius effect on this phase. The solid-state reaction route was utilized to prepare $(Tl_{0.6}Bi_{0.4})Sr_2(Ca_{1-x}Cd_x)Cu_2O_{7-\delta}$ (Tl-1212) with x = 0 to 0.20. Tl-1212 was dominant as indicated by x-ray diffraction patterns. The x = 0.15 sample showed the highest onset temperature $T_{c\text{-}onset}$ (95 K). The peak temperature, T_p of χ'' (imaginary part of the AC susceptibility) decreased pronouncedly with Cd content indicating weakening of inter-grain coupling. Cd substitution reduced the 2-dimensional to 3-dimensional conductivity transition from 139 K (x = 0) to 135 K (x = 0.15). From Lawrence-Doniach model it was shown that the sample with the highest $T_{c\text{-}onset}$ (x = 0.15) exhibited the shortest coherence length, highest anisotropy (γ = 9.692) and weakest inter-layer coupling (J = 0.421). Cd substitution lowers both the inter-layer and inter-grain coupling. These factors are important in optimizing the superconductivity of the Tl-1212 phase.

Keywords: Tl-1212 phase; Cd substitution; coherence length; inter-layer coupling; inter-grain coupling

1. INTRODUCTION

The effect of elemental substitution and addition on $TlSr_2CaCu_2O_7$ superconductor is an interesting research topic [1, 2]. RE^{+3} (rare earth) substitutions for Ca^{+2} in $TlSr_2CaCu_2O_7$ showed transition temperature, T_c of 90 K [3]. The T_c of $(Tl,Bi)Sr_2CaCu_2O_7$ is around 75-95 K [4] while $(Tl,Pb)Sr_2CaCu_2O_7$ has T_c around 85 K [5]. Pb, Bi, Cr and RE^{+3} substitutions stabilize the $TlSr_2CaCu_2O_7$ phase and improved T_c [6,7]. Cr and Pb are reported to have valency +3 [6] and +4 [5], respectively and Bi is report to be in the mixed $Bi^{+3/+5}$ state [4].

Copper oxide based superconductor (HTSC) including $TlSr_2CaCu_2O_7$ shows high anisotropy which gives rise to fluctuations in the conductivity. This fluctuation is also due to the short coherence length along the *c*-axis, $\xi_c(0)$. Above T_c, the resistivity vs. temperature curve deviates from linearity as a result of enhanced superconducting fluctuations [8]. The Lawrence-Doniach (LD) and Aslamazov-Larkin (AL) models can be used to analyze these fluctuations. Excess conductivity can be determined by subtracting the normal state conductivity from the measured value [9]:

$$1/\Delta\sigma = 1/\rho_{mea} - 1/\rho_{bk} \quad (1)$$

where ρ_{mea} is the experimental resistivity, $\rho_{bk} = \alpha + \beta T$, α is the resistivity at 0 K, and β is the derivative of the resistivity with respect to *T*. From AL and LD models [9-12], Δσ can be written as [9]:

$$\Delta\sigma/\sigma_o = A\varepsilon^{-\lambda} \quad (2)$$

where σ_o is the conductivity at 300 K and ε is the reduced temperature [13]:

$$\varepsilon = \ln (T/T^p_c) / T^p_c . \quad (3)$$

In the above equation the peak temperature T^p_c is obtained from dρ/dT and *A* is a constant. λ is calculated from the slope of $\ln(\Delta\sigma/\sigma_o)$ versus ln(ε) and is related to the conduction dimensionality D where λ = 2 - D/2. For 1-dimensional (1D), 2D and 3D regions, λ = 1.5, 1.0 and 0.5, respectively. Changes in $T_{2D\text{–}3D}$ and coherence length can be observed with substitution [14]. The LD model can be use to determine $T_{2D\text{–}3D}$ and $\xi_c(0)$ for polycrystalline samples by using [13]:

$$T_{2D\text{–}3D} = T_c\,[1 + (2\,\xi_c(0)/d)^2] \quad (4)$$

where *d* =3.18 Å is the interlayer distance of Tl-1212. Inter-layer coupling, *J* can be obtained from LD model [15]:

$$J = [2\,\xi_c(0)\,]^2/d^2 \quad (5)$$

The anisotropy, γ is written as [16]:

$$\gamma = \xi_{ab}(0) / \xi_c(0). \quad (6)$$

The coherence length is between 10 and 20 Å for HTSCs [13]. A transition from 2D to 3D with lowering temperature was observed in (Cu, Tl)-based superconductor [17–19]. Excess conductivity of $Tl_2Ba_2CaCu_2O_{8+d}$ (Tl-2212) [20-21] and TlSrCaCuO [22-24] has also been reported.

This paper is on the effect of Cd substitution in $(Tl_{0.6}Bi_{0.4})Sr_2(Ca_{1-x}Cd_x)Cu_2O_{7-\delta}$ (x = 0 - 0.20). Cd was chosen to partially replace Ca because both are single valence (+2). The ionic radius of Cd^{+2} with coordination number (CN) 4 to 12 (0.78-1.31 Å) overlaps with Ca^{+2} with CN 6 to 12 (1.00 - 1.34

Å). This substitution may not change the carrier concentration but instead lattice changes are expected. We report the electrical resistance (dc) measurements and X-ray diffraction patterns. AC susceptibility measurements are also reported together with changes in inter-grain coupling with Cd substitution. AL model was used to determine λ while LD model was employed to determine $\xi_c(0)$, J and γ.

2. EXPERIMENTAL DETAILS

$(Tl_{0.6}Bi_{0.4})Sr_2(Ca_{1-x}Cd_x)Cu_2O_{7-\delta}$ (Tl-1212) with x = 0, 0.05, 0.10, 0.15, 0.18 and 0.20 were fabricated through the solid-state reaction route. Metal oxides and carbonates (SrO, CaO, $CdCO_3$ and CuO) with purity ≥ 99.99 % were mixed and ground. The mixed powders were then heated at 900 ºC for a total of 48 h with intermediate grindings. Tl_2O_3 and Bi_2O_3 were added to the powders and pressed into pellets (13 mm diameter × 2 mm thickness). Excess Tl_2O_3 (10 %) was added to compensate for the loss during heating. A tube furnace was preheated to 1000 ºC after which the pellets were heated for 4 min in flowing O_2 and furnace cooled.

The four-probe method with silver paste contacts was used to determine the electrical resistance. For temperature dependent measurements, a Cryogenics Closed Cycle Refrigerator Model 22 from CTI was used. The onset transition temperature, $T_{c\text{-onset}}$ is the temperature where there is a sudden drop in resistance. The temperature where the resistance drops to zero is the zero-resistance temperature, $T_{c\text{-zero}}$.

A diffractometer from Bruker (D8 Advance) with a CuK_α source was utilized to determine the resultant phase. In order to calculate the lattice parameters 15 diffraction peaks were used. The volume fractions of each phase were calculated using [23, 24]:

$$\text{Tl}-1212(\%) = \frac{\sum I_{1212}}{\sum I_{1212} + \sum I_{1201}} \times 100\% \qquad (5)$$

$$\text{Tl}-1201(\%) = \frac{\sum I_{1201}}{\sum I_{1212} + \sum I_{1201}} \times 100\% \qquad (6)$$

where I_{1212} *and* I_{1201} is the intensity of the 1212 and 1201 phase, respectively.

Energy Dispersive X-Ray Analysis (EDX) using an Oxford Instrument analyser was used to determine the chemical composition of individual phases. A Cryo Industry AC susceptometer (REF-1808-ACS) with frequency = 295 Hz and magnetic field H = 5 Oe was used. The inter-grain critical current density $J_c(T_p)$ was calculated using the Bean's model [25], $J_c(T_p) = H/\sqrt{lw}$, where H is the magnetic field, and l and w is the dimension of the bar-shaped sample. T_p is the temperature where the imaginary part of the susceptibility χ" shows a peak.

3. RESULTS AND DISCUSSION

The x-ray diffraction patterns of all samples indicated that the Tl-1212 phase (tetragonal unit cell and space group, P4/mmm) was dominant (Figure 1).

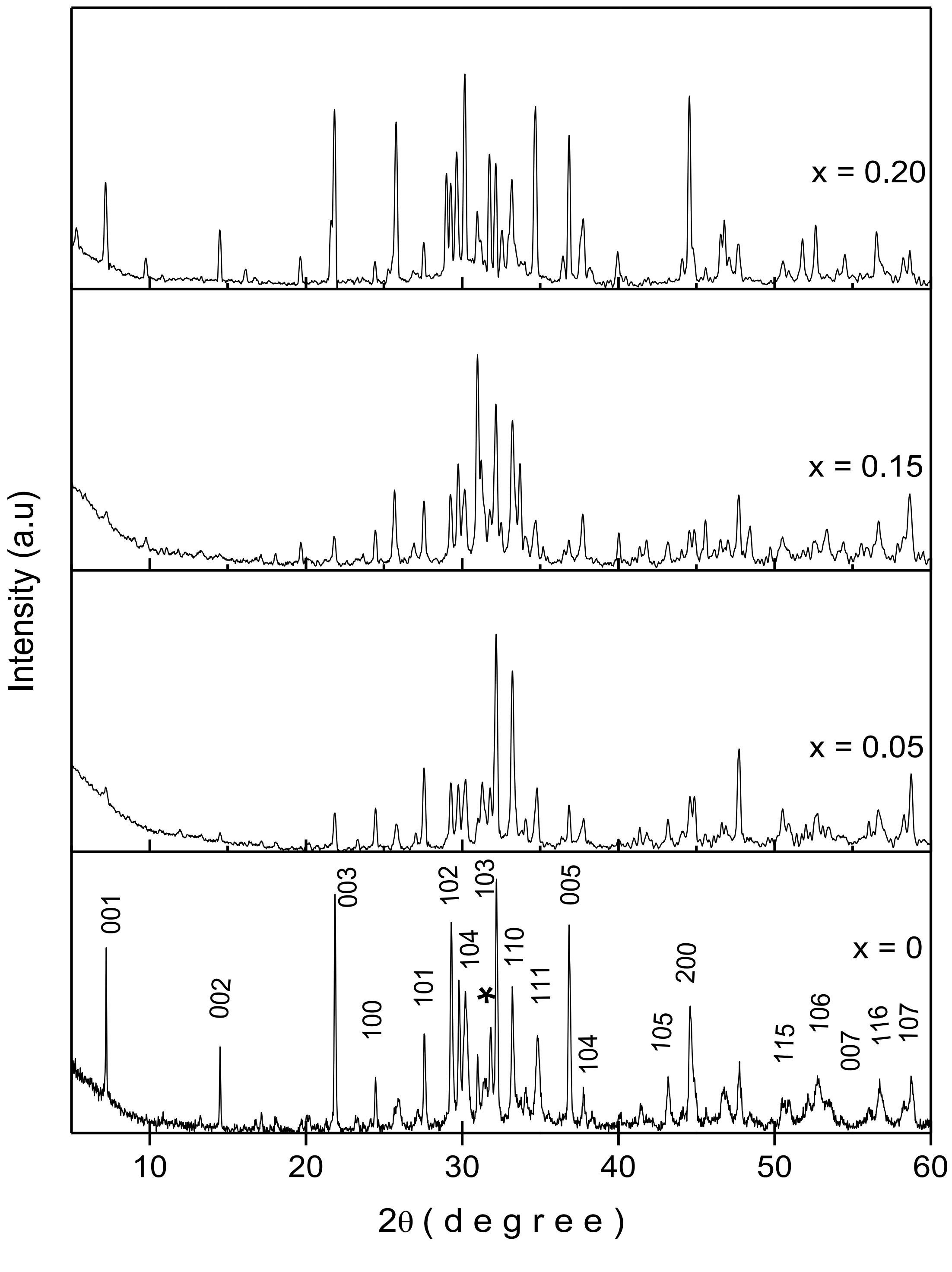

Figure 1. Powder X-ray diffraction patterns for $(Tl_{0.6}Bi_{0.4})Sr_2(Ca_{1-x}Cd_x)Cu_2O_{7-\delta}$ (x = 0, 0.05 0.10, 0.15, 0.18 and 0.20) showing major Tl-1212 phase. The 1201 phase is indicated by (*).

Table 1. Lattice parameters, $T_{c\text{-}onset}$, $T_{c\text{-}zero}$, room temperature resistivity (ρ_{297}), $T_{c\chi'}$, T_p, $J_c(T_p)$, T^p_c, α, β, $T_{2D\text{-}3D}$, λ_{2D}, λ_{3D}, $\xi_c(0)$, J and γ for x = 0 to 0.15

x	0	0.05	0.1	0.15
a (Å) ± 0.003	3.800	3.802	3.809	3.805
c (Å) ± 0.005	12.002	12.033	12.047	12.187
$T_{c\text{-}onset}$ (K)	94	94	87	95
$T_{c\text{-}zero}$(K)	86	84	43	80
ρ_{297} (mΩcm)	8.63	7.00	16.7	109
T^p_c(K)	88	85	62	83
$T_{c\chi'}$(K)	93	90	-	86
T_p(K)	70	67	-	45
$J_c(T_p)$ (A/cm^2)	42	12	-	11
$\alpha = \rho_n$(0K)(mΩcm)	0.4	2.8	9.2	56
$\beta = d\rho/dT \times 10^{-3}$				
(mΩcm)/K	2.91	3.06	3.26	5.93
$T_{2D\text{–}3D}$ (K)	139	137	-	135
λ_{2D}	1.005	0.933	-	0.885
λ_{3D}	0.478	0.474	0.473	0.470
J	0.478	0.457	-	0.421
$\xi_c(0)$ (Å)	1.100	1.075	-	1.032
γ	9.090	9.298	-	9.692

Diffraction peaks from $TlSr_2CuO_5$ (Tl-1201) phase were also observed in some samples. The x = 0.05 sample showed the highest Tl-1212 volume fraction. $T_{c\text{-}onset}$, $T_{c\text{-}zero}$, resistivity (at 297 K), and a and c lattice parameters are shown in Table 1 where a and c increased with Cd substitution.

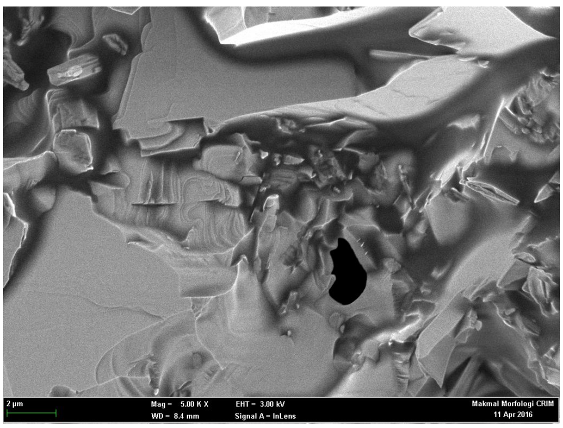

A

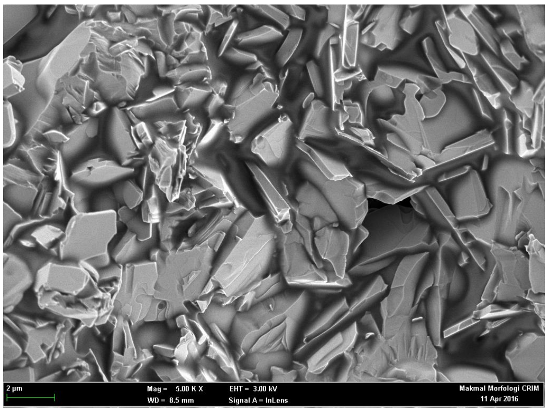

B

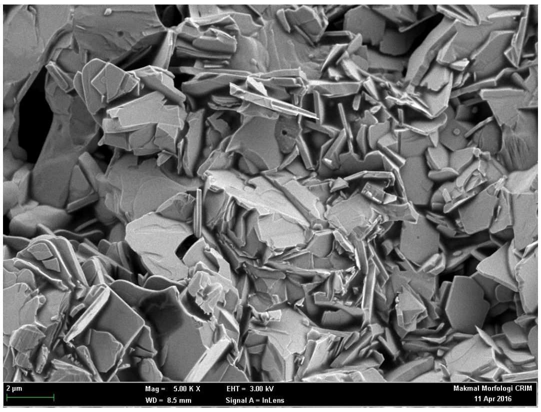

C

Figure 2. SEM micrographs for (a) x = 0, (b) x = 0.05 and (c) x = 0.15

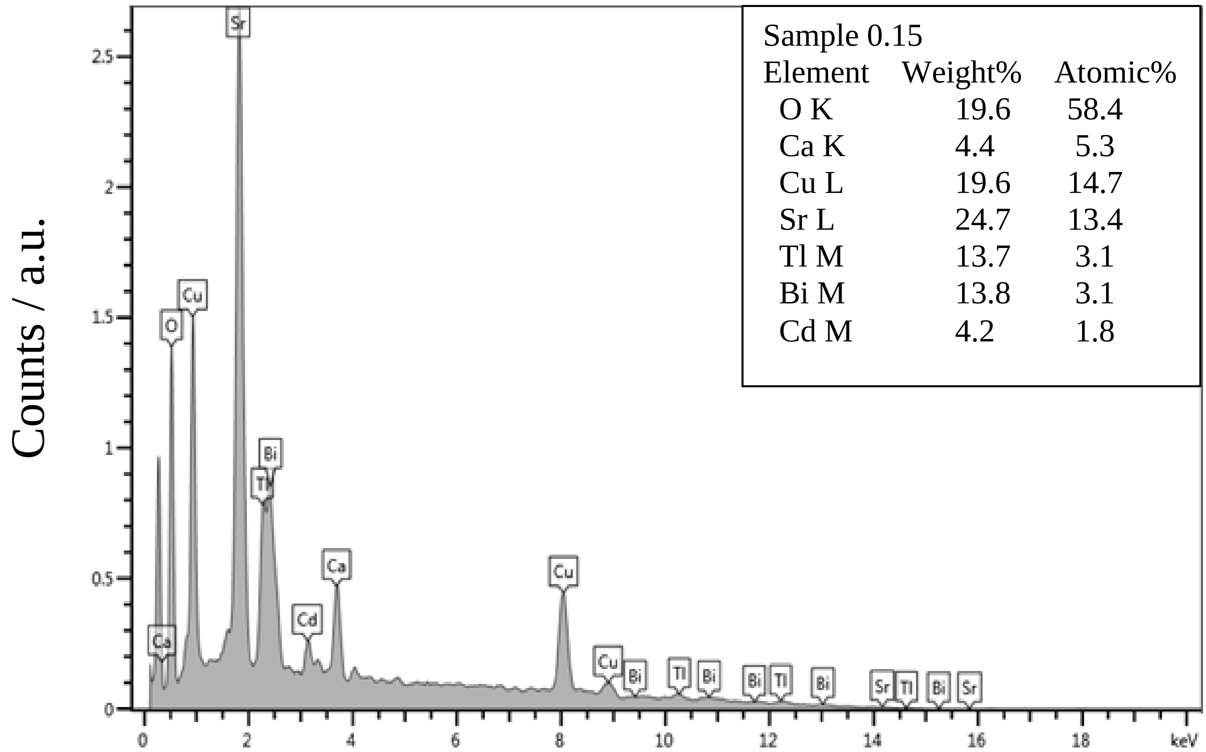

Figure 3. EDX spectrum for x = 0.15, insert shows the weight percent for each element

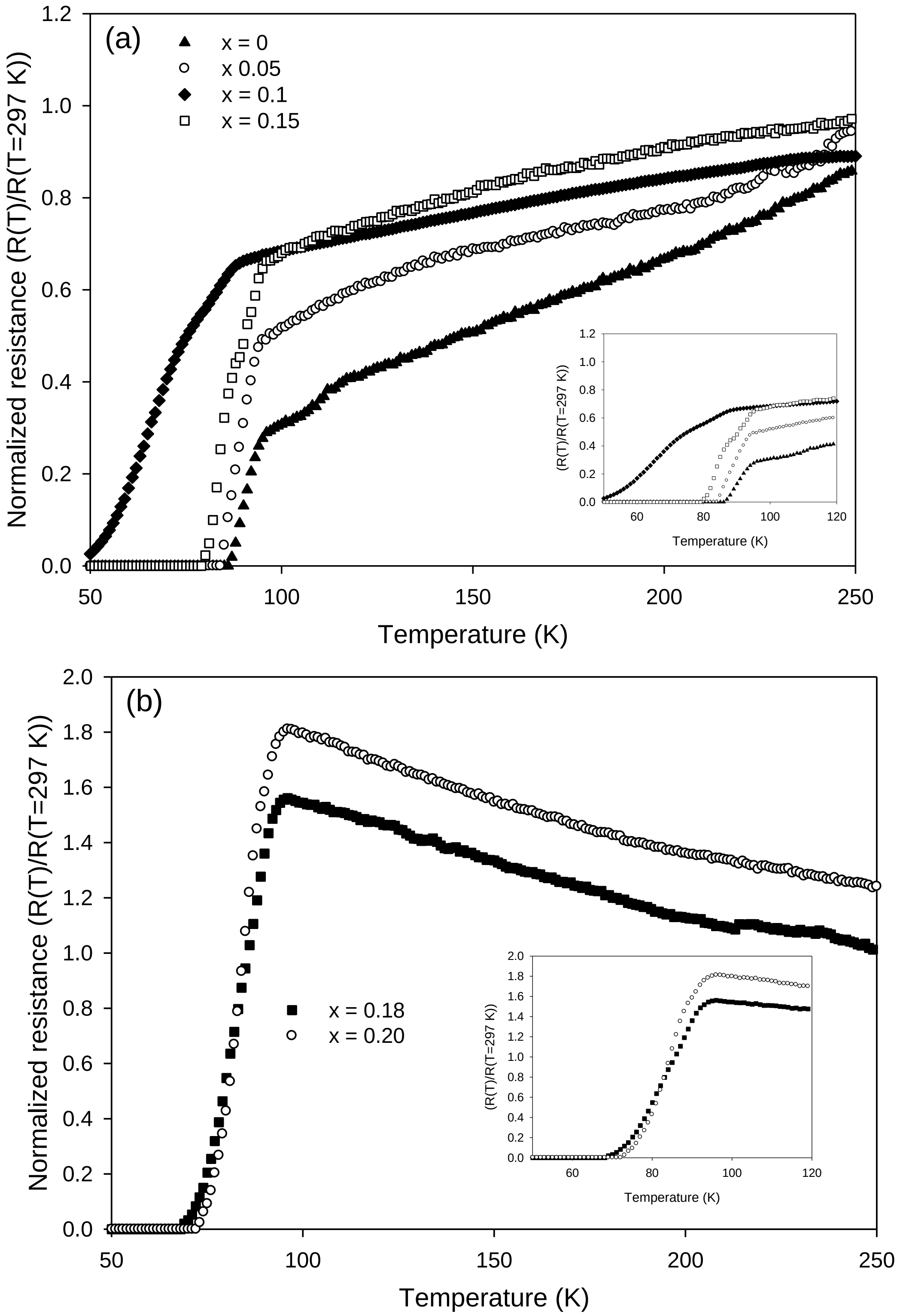

Figure 4. (a) Normalized resistance ($R/R_{(T=297)}$) versus temperature curves of $(Tl_{0.6}Bi_{0.4})Sr_2(Ca_{1-x}Cd_x)Cu_2O_{7-\delta}$ for x = 0, 0.05,0.10 and 0.15 and (b) x = 0.18 and 0.20.

The microstructure of the x = 0 sample showed a smooth surface with minor voids (Figure 2(a)). Substitution of Cd resulted in randomly oriented plate-like grains (≈ 2μm) (Figure 2(b) and

2(c)). The EDX spectrum of x = 0.15 samples is shown in Figure 3. Insert shows the composition of the x = 0.15 sample indicating percentage of elements similar to the Tl-1212 phase with minor deviation as a result of the Tl-1201 phase.

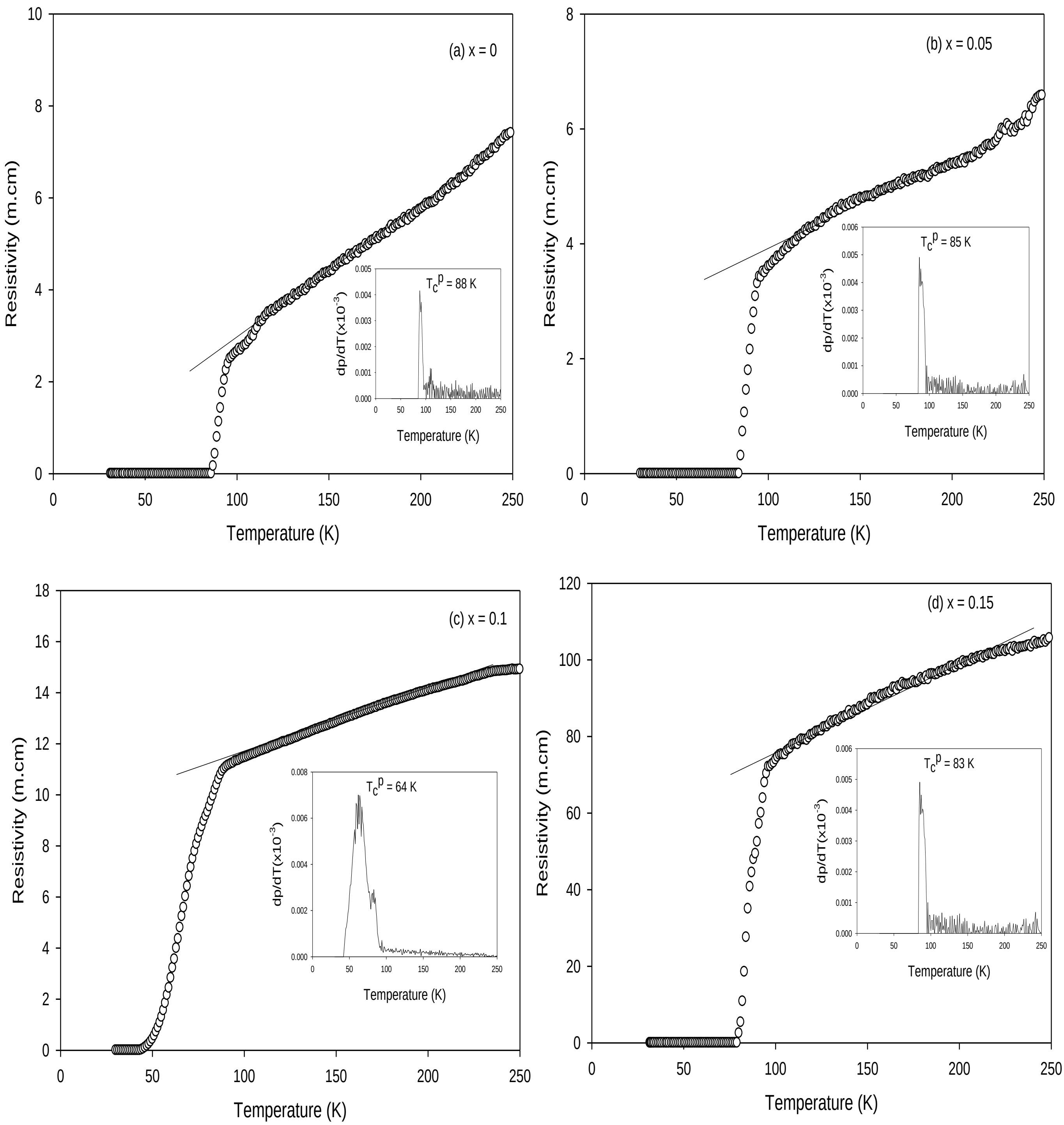

Figure 5. Electrical resistivity of $(Tl_{0.6}Bi_{0.4})Sr_2(Ca_{1-x}Cd_x)Cu_2O_{7-\delta}$ (x = 0, 0.05, 0.10, 0.15, 0.18 and 0.20) samples. The linear fit shows the background normal state resistivity projection. Inset shows plots of dρ/dT versus temperature.

The electrical resistance vs. temperature curves showed that the x = 0.15 sample exhibited the highest $T_{c\text{-onset}}$ (95 K) (Figure 4). Samples with $0 \leq x \leq 0.15$ exhibited a linear metallic behavior while the sample with $x \geq 0.18$ showed semiconductor-like behavior. The ratio of the lattice parameter a/c indicates the internal lattice strain.

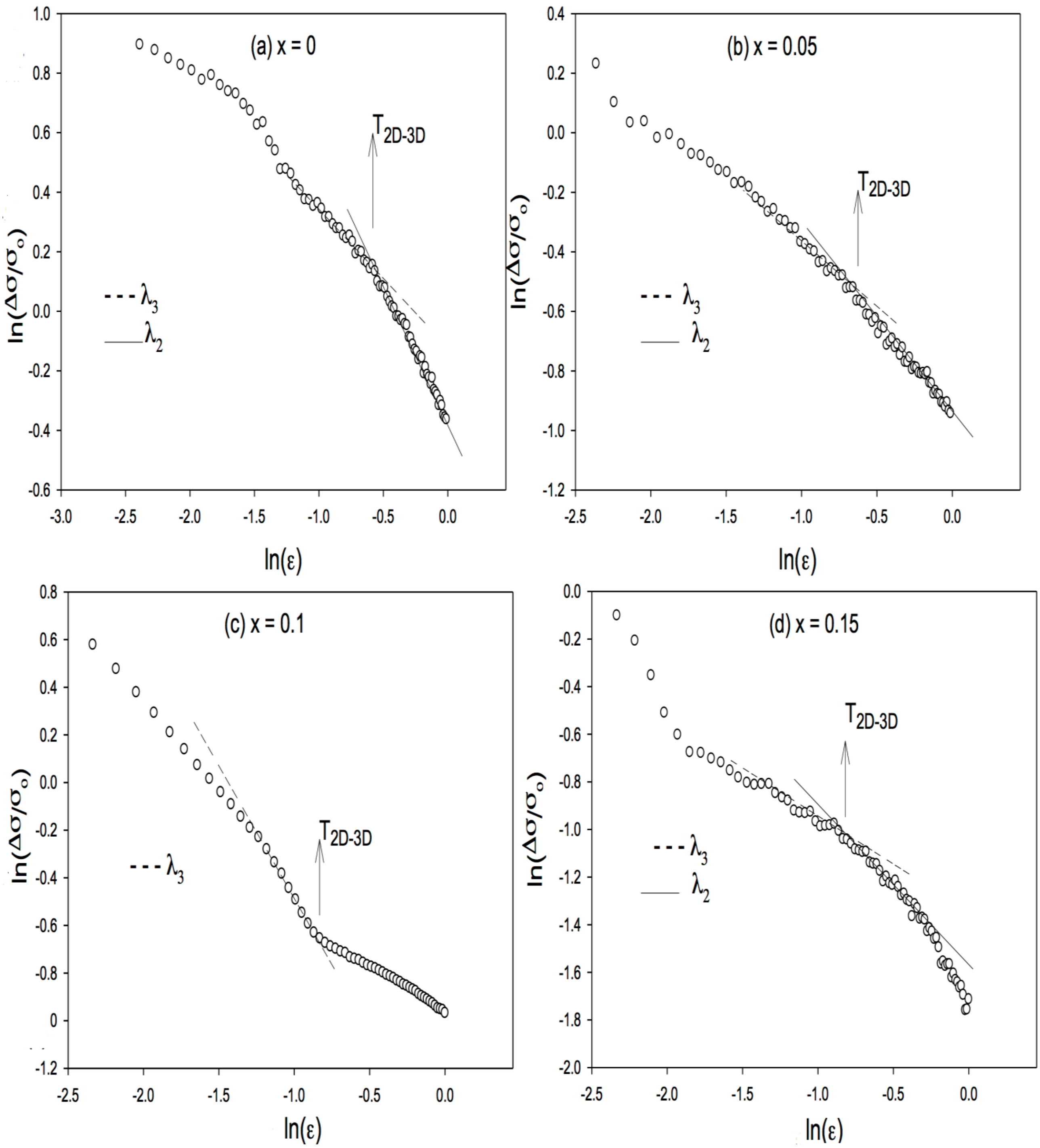

Figure 6. Plot of $\ln(\Delta\sigma/\sigma_o)$ versus $\ln(\varepsilon)$ of $(Tl_{0.6}Bi_{0.4})Sr_2(Ca_{1-x}Cd_x)Cu_2O_{7-\delta}$ x = 0, 0.05, 0.10 and 0.15) samples. The solid line represents the 2-D and dotted line 3-D theoretical slope.

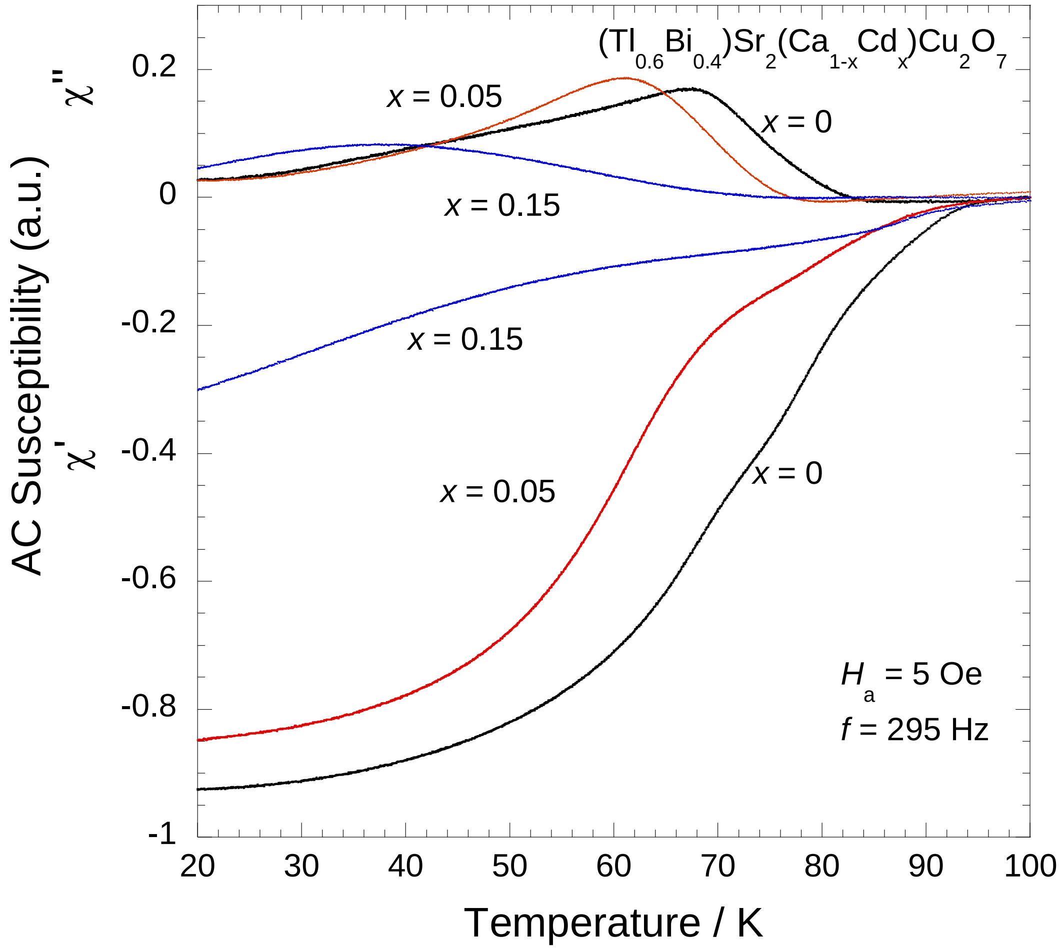

Figure 7. AC susceptibility measurements of $(Tl_{0.6}Bi_{0.4})Sr_2(Ca_{1-x}Cd_x)Cu_2O_{7-\delta}$ $x = 0$, 0.05 and 0.15

The ratio a/c of $x = 0$, 0.05, 0.01 and 0.15 are 0.3166, 0.3160, 0.3162 and 0.3122, respectively. The increase in the transition temperature of the $x = 0.15$ sample can be attributed to the changes in the internal lattice strain and hence the chemical pressure in the Tl-1212 unit cell. A similar change in T_c with change in lattice strain was also observed in $YBa_2Cu_{3(1-x)}Al_{3x}O_x$ [26].

The electrical resistivity fittings to $\rho = \alpha + \beta T$ showed deviation from linear behavior (Figure 5) due to superconducting fluctuations. The peak temperature ($T^p{}_c$) of $d\rho/dT$ was used to determine the reduced temperature, ε. The $x = 0$ to 0.15 samples showed a single peak which indicated that the transition occurs within grains. Figure 5 shows plots of $\ln(\Delta\sigma/\sigma_o)$ vs. $\ln(\varepsilon)$ of $x = 0$, 0.05, 0.10 and 0.15. The solid line indicates the 2-dimensional and the dashed line indicates 3-dimensional (theoretical) slope.

Graphs of $\ln(\Delta\sigma/\sigma_o)$ versus $\ln(\varepsilon)$ were plotted and the experimental versus the theoretical curves showed that the fluctuation was in the mean field regime: $-3 < \ln(\varepsilon) < 1$ (Figure 6). A transition from 2D to 3D was observed with decreasing temperature. Table 1 shows $T^p{}_c$, α, β $T_{2D\text{-}3D}$, $\xi_c(0)$, J and γ for the samples. β changed from 19.71×10^{-3} to 34.84×10^{-3} (mΩ-cm)/K as x was changed from 0 to 0.2. 2D- to 3D transitions was observed as a result of Cd substitution for Ca. Our analyses also showed the dependence of $\xi_c(0)$ on Cd. For $x = 0.15$, $\xi_c(0)$ indicated the highest anisotropy among all samples. Cd substitution caused lowering of T_{2D-3D} and the $x = 0$ sample showed the highest T_{2D-3D}. A decrease in inter-layer coupling J with Cd substitution was also observed. This weakening of inter-layer coupling may cause the variations in $T_{c\text{-onset}}$. In our samples the inter-layer coupling $J < 1$ indicating a weak coupling between the copper oxide planes. Our results showed that the partial substitution of Ca^{2+} by Cd^{2+} weakens the copper oxide inter-layer coupling. Previous reports also indicated inter-layer coupling $J < 1$ in the Tl-based samples [8,13]. The coherence length for our samples at 0 K, $\xi(_c0)$ is about 1 Å which is consistent with previously reported values in Tl-1212 [8] and $CaREBa_2Cu_3O_7$ (RE=La and Sm) [27].

In Table 2 we make comparison with $(Tl_{0.5}Pb_{0.5})Sr_{1.8}Yb_{0.2}(Ca_{1-x}Mg_x)Cu_2O_{7-\delta}$ [13]. This series also showed that the sample with the highest $T_{c\text{-onset}}$ ($x = 0.6$) exhibited the highest anisotropy γ, lowest inter-layer coupling J, shortest coherence length $\xi_c(0)$ and lowest λ_{2D}. Hence, these factors are important in determining and optimizing T_c of the Tl-1212 superconductors. In Cu substituted Tl-1212 samples FTIR data showed that T_c was suppressed with increase in coupling of CuO_2 planes [14] and this result is consistent with our findings on the relation between inter-layer coupling and superconducting transition.

Table 2. $T_{c\text{-onset}}$, λ_{2D}, λ_{3D}, $\xi_c(0)$, J and γ for our samples $(Tl_{0.6}Bi_{0.4})Sr_2(Ca_{1-x}Cd_x)Cu_2O_{7-\delta}$, and $(Tl_{0.5}Pb_{0.5})Sr_{1.8}Yb_{0.2}(Ca_{1-x}Mg_x)Cu_2O_{7-\delta}$ [13]

	$T_{c\text{-onset}}$	λ_{2D}	λ_{3D}	$\xi(_c0)$	J	γ
$(Tl_{0.6}Bi_{0.4})Sr_2(Ca_{1-x}Cd_x)Cu_2O_{7-\delta}$						
0	94	1.005	0.478	1.100	0.478	9.090
0.05	94	0.933	0.474	1.075	0.457	9.298
0.15	95	0.885	0.470	1.032	0.421	9.692
$(Tl_{0.5}Pb_{0.5})Sr_{1.8}Yb_{0.2}(Ca_{1-x}Mg_x)Cu_2O_{7-\delta}$						
0	107.3	1.079	0.439	0.43	0.073	23.3
0.2	107.6	1.088	0.476	0.49	0.095	20.4
0.4	108.6	0.976	0.479	0.70	0.194	14.3
0.6	109.6	0.968	0.538	0.26	0.027	38.5

AC susceptibility shows that the transition temperature ($T_{c\chi'}$) was between 86 K and 93 K (Figure 7). The decrease in χ' of the complex susceptibility ($\chi = \chi' + i\chi''$) below the susceptibility transition temperature, $T_{c\chi'}$ indicates the start of diamagnetic properties and peak in χ'' (T_p) represents AC losses. T_p shifts depending on the pinning force strength. The weaker the pinning, the larger is the shift to the left in the maximum of χ''. Below T_p the amplitude of χ'' falls due to the decrease in flux penetration. All of our samples showed a single peak in χ'' ($H = 5$ Oe) and this is consistent with previously reported results on $Tl_{0.8}Pb_{0.4}Sr_{1.8}Ba_{0.2}Ca_2Cu_3O_x$ for measurement at $H = 4$ Oe [28].

The inter-grain critical current density at T_p, $J_c(T_p)$ decreased with Cd substitution i.e. J_c (T_p = 70 K) = 42 A/cm^2 for $x = 0$ to J_c (T_p = 45 K) = 11 A/cm^2 for $x = 0.15$. This result showed that Cd suppressed the inter-grain coupling. The peak temperature T_p decreased from 70 K ($x = 0$) to 67 K (x = 0.05). This showed that the full flux penetration occurred at lower temperature as Cd was added. Changes in the microstructure (Figure 2) to smaller grain size also contributed to this decrease. Table

1 shows $T_{c\text{-}onset}$, $T_{c\chi'}$, T_p and $J_c(T_p)$ for x = 0, 0.05 and 0.15 samples.

In conclusion, excess conductivity analysis of $(Tl_{06}Bi_{0.4})Sr_2(Ca_{1-x}Cd_x)Cu_2O_{7-\delta}$ showed that 2D to 3D transition temperature was lowered with Cd substitution. The x = 0.15 sample which showed the highest $T_{c\text{-onset}}$ exhibited the weakest inter-layer coupling (J = 0.421) and the highest anisotropy (γ = 9.692). Moreover, Cd substitution caused a decrease in T_{2D-3D} to lower temperatures. $T_{c\chi'}$ did not change very much with Cd addition. However, T_p was severely suppressed indicating weakening of inter-grain coupling as Cd was substituted. This work showed that Cd substitution weakened the inter-layer coupling and also the inter-grain coupling. These factors are important considerations in optimizing the Tl-1212 phase.

ACKNOWLEDGEMENTS
We thank the Ministry of Higher Education, Malaysia for supporting this work under grant number FRGS/1/2017/STG02/UKM/01/1.

References

1. G. Gritzner, H. Sudra, H. Gabriel, V. Kavecanský and J.L. Soubeyroux, *Superconductor Science Technology,* 21 (2008) 125009.
2. R. Abd-Shukor and A. D. Arulsamy, *Journal of Physics D*, 33 (2000) 836.
3. Z.Z. Sheng, Y. Xin, D.X. Gu, J.M. Meason, J. Bennett, D. Ford and D.O. Pederson, *Physica B*, 84 (1991) 349.
4. S. Li and M. Greenblatt, *Physica C*, 157 (1989) 365.
5. M.A. Subramaniam, C.C. Torardi, J. Gopalakrishnan, P.L. Gai, J.C. Calabrese, T.R. Askew, R.B. Flippen and A.M. Sleight, *Science,* 242 (1988) 249.
6. Z.Z. Sheng, D.X. Gu, Y. Xin, D.O. Pederson, L.W. Finger, C.G. Hadidiacos and R.M. Hazen, *Physics Letter B*, 5 (1991) 635.
7. R.S. Liu, J.M. Liang, Y.T. Huang, W.N. Huang, S.F. Wu, H.S. Koo, P.T. Wu and L.J. Chen, *Physica C*, 162 (1989) 869.
8. S. Ismail, A.K. Yahya and N.A. Khan, *Ceramics International*, 39 (2013) S257.
9. T. Sato, H. Nakane, N. Mori and S. Yoshizawa, *Physica C*, 357–360 (2001) 244.
10. L.G. Asmalazov and A.L. Larkin, *Physics Letter A*, 26 (1968) 238.
11. W.E. Lawrence and S. Doniach, P*roceedings of the 12th International Conference on LowTemperature*. in: Eizo Kanda (Ed.), Physics, Keigaku. Tokyo, 1971, p. 361.
12. A. Al-Sharabi and R. Abd-Shukor, *Journal of Alloys and Compounds,* 615 (2014) 363.
13. A. Ali Yusuf, A.K. Yahya, N.A. Khan, F. Md. Salleh, E. Marsom and N. Huda, *Physica C*, 471 (2011) 363.
14. N.H. Ahmad, N.A. Khan and A.K. Yahya, *Journal of Alloys and Compounds,* 492 (2010) 473.
15. N.A. Khan and A. Mumtaz, *Physica B*, 404 (2010) 2772.
16. N.A. Khan, N. Hassan, M. Irfan and T. Firdous, *Physica B*, 405 (2010) 1541.
17. N.A. Khan and M. Irfan, *Physica C*, 468 (2008) 2341.
18. N.A. Khan and G. Husnain, *Physica C,* 436 (2006) 51.
19. N.A. Khan, A.A. Khurram and A. Maqsood, *Physica C*, 398 (2003) 114.
20. H.M. Duan, W. Kiehl, C. Dong, A.W. Cordes, M.J. Viar, D.L. Saeed and A.M. Hermann, *Physical Review B*, 43 (1991) 12925.

21. D.H. Kim, K.E. Gray and M.D. Trochet, *Physical Review B*, 45 (1992) 10801.
22. N. Huda, A.K. Yahya and W.F. Abdullah, *AIP Conference Proceedings*, 1017 (2008) 114.
23. N. Huda and A.K. Yahya, *Materials Research and Innovations*, 13 (2009) 3.
24. N.H. Ahmad, N.A. Khan and A.K. Yahya, *Journal of Alloys and Compounds*, 492 (2010) 473.
25. C.P. Bean, *Review of Modern Physics*, 36 (1964) 31.
26. Yuhuan Xu, Zhongrol Gi, Chaorui Li, Xianduan Lin, Wi Li, Wanming Lao, Hong Wang and Guowei Chen, *Phys. Stat. Sol.* (a)109 (1988) 301.
27. H. Krishnan, R. Srinivasan, V. Sankaranarayanan, C. K. Subramaniam and G. V. Subba Rao, *Bull. Mater. Sci.* 14 (1991) 747.
28. J.H. Lee, R. Baek, G.C. Kim, Y.C. Kim and D.Y. Jeong, *Physica C* 402 (2004) 347.

© 2018 The Authors. Published by ESG (www.electrochemsci.org). This article is an open access article distributed under the terms and conditions of the Creative Commons Attribution license (http://creativecommons.org/licenses/by/4.0/).